Special Section: Patterns

Gonzalo Martínez*
Karl Vanderlinden
Juan Vicente Giráldez
Antonio J. Espejo
José Luis Muriel

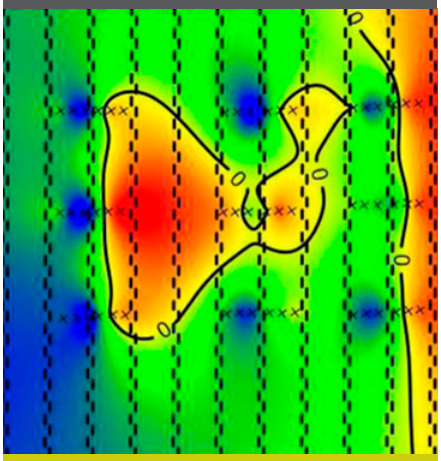

Spatiotemporal variability of apparent electrical conductivity measured in a clay soil with various soil management systems, is explained in terms of soil moisture, topography, and tillage patterns. Time-lapse images of apparent electrical conductivity show the field response to the interplay between rainfall, soil surface state, and soil profile properties.

G. Martinez, K. Vanderlinden, A. Espejo and J.L. Muriel, IFAPA, Centro Las Torres-Tomejil, Ctra. Sevilla-Cazalla km 12.2, 41200 Alcalá del Río, Sevilla, Spain; J.V. Giráldez, Dep. de Agronomía, Univ. de Córdoba, Campus de Rabanales, Edificio da Vinci. Ctra. Madrid, km 396, 14071 Córdoba, and Instituto de Agricultura Sostenible, CSIC, Avda. Menéndez Pidal, s/n, 14080 Córdoba, Spain. *Corresponding author (z42magag@uco.es).

Vadose Zone J. 9:871–881
doi:10.2136/vzj2009.0160
Received 13 Nov. 2009.
Published online 20 Oct. 2010.



# Field-Scale Soil Moisture Pattern Mapping using Electromagnetic Induction

Soil apparent electrical conductivity ($EC_a$) responds to time-variable soil properties, such as soil water content (θ), and can therefore be used to characterize the spatial and temporal dynamics of θ at the field scale. When clay content is high and uniform and the θ range small, however, it is not clear whether $EC_a$ maps can be used for this purpose. A soil management experiment established in a Vertisol in 1982 was surveyed for $EC_a$ on 13 occasions to capture changing soil conditions and to determine the sources of this variability. Less variation with time was found in subsoil than in topsoil $EC_a$ patterns, especially within the conventional tillage (CT) plots, in areas with shallow soil, and along the drainage network. Using the 13 $EC_a$ relative difference data sets as variables, principal component (PC) analysis showed that the first three PCs explained 90% of their total variance. The time-stable or mean $EC_a$ pattern was significantly correlated with PC1 and could also be associated with topography, soil depth, and soil structure but could not be related to a single survey. Topography and soil management could be associated with PC2 and PC3, respectively. Time-stable θ patterns, inferred from 26 surveys, revealed topographical and management characteristics and showed significant relationships ($P < 0.001$) with $EC_a$–derived patterns like soil porosity and infiltration caused by soil management, topography, and rainfall. Electromagnetic induction sensors were useful for mapping soil spatial variability and changing soil conditions due to management effects and external forcing in uniform clay soils.

Abbreviations: CT, conventional tillage; DD, direct drilling; $EC_a$, apparent electrical conductivity; $EC_{ad}$, deep apparent electrical conductivity; $EC_{as}$, shallow apparent electrical conductivity; MT, minimum tillage; PC, principal component; PCA, principal components analysis.

**Soil water content** controls most biogeochemical fluxes within and between the soil, plants, and the atmosphere and can therefore be considered as the link between the energy, water, and C cycles (Rodriguez-Iturbe, 2000). A better knowledge of θ patterns could improve our understanding of these fluxes and enhance our capacity to characterize their behavior at the field or catchment scale (Vereecken et al., 2008). Accurate soil moisture measurement across spatial and temporal scales is still a challenging task (Robinson et al., 2008), however. Especially at intermediate spatial (0.1–100 ha) and temporal (minutes to days) scales, a data gap remains that limits our understanding of interactions among the processes that govern the (eco)hydrologic response of small watersheds (Western et al., 2002). The combination of emerging near-surface hydrogeophysical imaging techniques (Robinson et al., 2008) and distributed wireless sensor networks (Bogena et al., 2009) can provide relevant hydrologic information and soil moisture data at these intermediate scales. Especially appealing is the possibility of using near-surface geophysical sensing data for downscaling remotely sensed θ or to characterize a priori time-stable θ patterns to guide the design of optimized monitoring networks without the need to first monitor θ during a determined period at a large number of locations (Guber et al., 2008).

Electromagnetic induction sensors, such as the EM38 (Geonics Inc., Mississauga, ON, Canada) provide noninvasive measurements of the soil $EC_a$, which depends on many soil properties. Friedman (2005) distinguished three categories, describing the bulk soil, solid particles, and the soil solution. Porosity, θ, and structure are factors contained within the first category, while particle shape and orientation, particle-size distribution, cation exchange capacity, and wettability belong to the second category and can generally be considered as time invariant. The electrical conductivity of the soil solution, cation composition, and temperature belong to the third category and change rapidly with time in response to environmental conditions (e.g., atmospheric forcing or soil management). A widely accepted model for $EC_a$ consists of adding up the contributions of the soil solution ($EC_w$), adjusted by θ for unsaturated conditions, and the adsorbed cations of the solid

phase ($EC_s$), representing roughly the time-variable and -invariable soil properties that affect $EC_a$, respectively (Rhoades et al., 1976; Mualem and Friedman, 1991). The contribution of the second term becomes increasingly important from coarse- to fine-textured soils and can explain the non-uniqueness of the $EC_a$–θ relations found in the literature. Because clay and organic matter content have a large effect on the soil hydraulic properties and soil moisture status, $EC_s$ is also expected to be spatially correlated with θ. It is therefore often not clear to what degree the observed $EC_a$–θ relations are only a consequence of the $EC_a$–clay content relation.

Kachanoski et al. (1988) found a second-order polynomial relationship between $EC_a$ and θ in a 1.5-ha field with a strong dependence of soil texture, $EC_a$, and θ on elevation, and clay and θ ranges of 41.5% and 0.30 $m^3\ m^{-3}$, respectively. Reedy and Scanlon (2003) and Robinson et al. (2009) found linear $EC_a$–θ relations, although the latter recognized that no single valid relationship could be determined for the entire study site. McCutcheon et al. (2006) fitted an exponential function to $EC_a$ and θ data from a 110-ha field with clay and sand content ranges of 20 and 45%, respectively, and a θ range of 0.23 $m^3\ m^{-3}$.

In these studies, the spatial variability of the clay content was sufficiently large to establish a significant relation with $EC_a$. Under these conditions, it can be expected that the range of θ values will also be large enough to infer a significant $EC_a$–θ relation. Uniform clay soils, such as Vertisols, often exhibit a small range of θ values on a single sampling date while clay dominates the contribution to $EC_a$ through the $EC_s$ term. It is not clear whether electromagnetic induction can provide relevant information about the spatial distribution of θ under these circumstances.

Another geophysical technique, ground-penetrating radar (GPR), is increasingly used for high-resolution θ mapping (Lambot et al., 2006; Weihermüller et al., 2007; Lambot et al., 2008). The method relies on the transmission and reception of electromagnetic waves through the soil. The propagation velocity of these waves, like other electromagnetic methods such as time domain reflectometry, depends on the soil dielectric permittivity, which is then related to θ (Topp et al., 1980). The drawbacks of this method are mainly a consequence of the dependence of the permittivity–θ relation on soil texture, temperature, electrical conductivity, and measurement frequency (Evett and Parkin, 2005), especially in soils containing clays with a high surface area and ion exchange capacity. In such soils, GPR wave propagation suffers attenuation, leading to reduced exploration depths and inaccurate determination of permittivity.

Within this context, the use of time-lapse $EC_a$ images seems a promising alternative, contrasting readings from $EC_a$ surveys under contrasting soil moisture conditions after a simple data transformation filters the contribution of the time-invariant properties ($EC_s$) to the $EC_a$ signal and elucidates patterns of time-variable properties. This technique was used successfully by Abdu et al. (2008), Martínez et al. (2009), and Robinson et al. (2009) to identify hydrologic subsurface patterns, soil texture, water-holding capacity, and θ patterns.

When a sequence of $EC_a$ surveys is available, independent underlying patterns can be inferred and associated with the possible sources of this spatial variability using principal component analysis (PCA). In addition, time-stable $EC_a$ patterns or areas of maximum and minimum temporal variability can be identified using temporal stability analysis (Vachaud et al., 1985). This information reveals spatial features that improve our understanding of the field-scale θ dynamics and help to decide on sensor location when implementing field-scale sensor networks.

The objectives of this study were (i) to evaluate the usefulness of electromagnetic induction for mapping field-scale θ patterns in a cropped uniform clay soil under contrasting soil management systems, (ii) to compare these patterns with time-stable θ patterns obtained through direct soil sampling, (iii) to identify and quantify the underlying sources of spatial variability in spatiotemporal $EC_a$ data, and (iv) to illustrate and discuss the combined effects of θ variation and soil management on $EC_a$ at the field scale under different environmental conditions.

# Materials and Methods

## Study Site

The $EC_a$ surveys were conducted at the Tomejil Farm long-term soil management experiment in southwest Spain (ltse.env.duke.edu/node/1191 [verified 31 July 2010]; 37°24′ N, 5°35′ W, 79 m above sea level), where the agronomic and environmental consequences of CT, direct drilling (DD), and minimum tillage (MT) have been compared since 1982. Four replicates of each treatment, with elemental plot dimensions of 15 by 180 m, are laid out in a completely random design within a 3.5-ha dryland field (Fig. 1A) under a wheat (*Triticum durum* L.)–sunflower (*Helianthus annuus* L.)–field pea (*Pisum sativum* L.) rotation. The soil is classified as a Chromic Haploxerert (Soil Survey Staff, 1999) with an increasing clay content toward the subjacent marl, ranging from 49 to 60, 49 to 64, and 53 to 65% in the 0- to 0.20-, 0.20- to 0.40-, and 0.40- to 0.60-m depths, respectively (Table 1), and an average organic C content of 10 $g\ kg^{-1}$. The clay content is high and quite homogeneous across the field, with a coefficient of variation <5% and without differences among the soil management systems (Table 1). The climate is Mediterranean, with an average annual rainfall of 495 mm, characterized by large intra- and interannual variability, and an average potential evapotranspiration ($ET_0$) of 1580 mm $yr^{-1}$. These conditions confer on the soil physical properties a high capacity to change with time as a consequence of contraction and expansion of the clay particles. During the study period, the crop sequence was sunflower–field pea–wheat–sunflower. Rainfall and $ET_0$ were measured at the site with an automatic weather station.

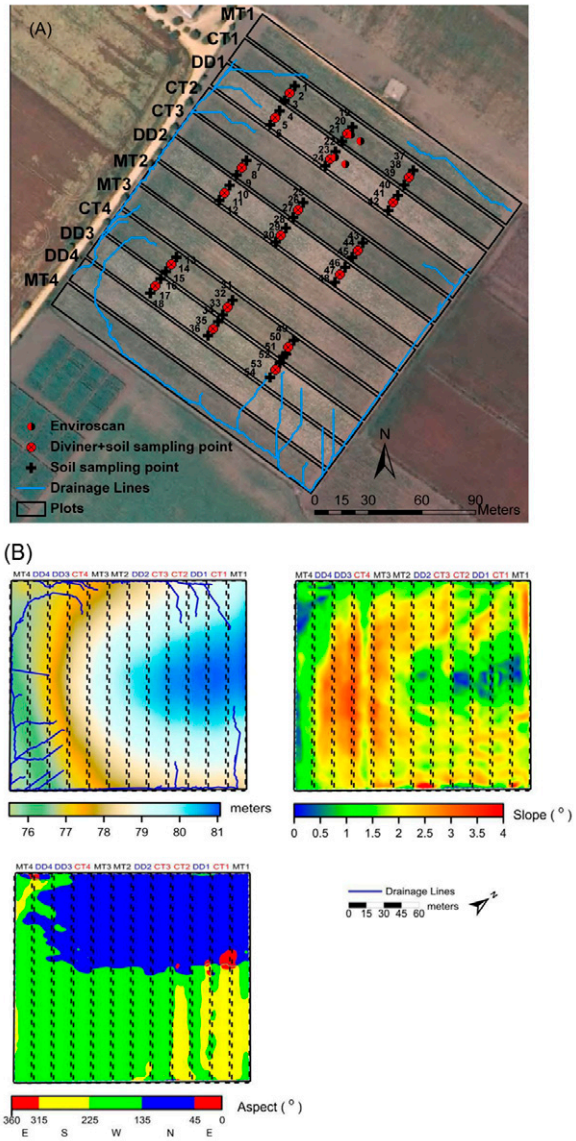


Fig. 1. (A) Map of the field with superposed plot limits, drainage network, location of 54 gravimetric soil sampling locations, four Enviroscan multisensory capacitance probes, and 18 Diviner single-sensor capacitance probe access tubes (MT, minimum tillage; CT, conventional tillage; DD, direct drilling); and (B) topographical maps of (from left to right) topography, slope, and aspect with superposed plot limits and drainage lines.

Table 1. Descriptive statistics of clay content and average (January 2008–March 2009) gravimetric soil moisture content ($\theta_g$) for each management system and sampling depth.

| | Conventional Tillage | | | | | |
|---|---|---|---|---|---|---|
| | $\theta_g$ | | | Clay content | | |
| Parameter | 0–0.10 m | 0.25–0.35 m | 0–0.35 m | 0–0.20 m | 0.20–0.40 m | 0.40–0.60 m |
| | % | | | | | |
| | Conventional Tillage | | | | | |
| Mean | 22.95 | 22.86 | 22.88 | 55.09 | 57.02 | 59.82 |
| SE | 0.17 | 0.17 | 0.18 | 0.51 | 0.71 | 0.55 |
| Median | 22.99 | 22.84 | 22.96 | 55.68 | 57.49 | 60.36 |
| Min. | 20.71 | 21.42 | 21.20 | 49.36 | 49.49 | 53.21 |
| Max. | 24.52 | 24.69 | 24.91 | 59.74 | 64.33 | 63.67 |
| SD | 0.91 | 0.86 | 0.93 | 2.67 | 3.70 | 2.86 |
| CV | 0.040 | 0.038 | 0.041 | 0.049 | 0.065 | 0.048 |
| Skewness | −0.245 | 0.399 | 0.181 | −0.416 | −0.093 | −0.776 |
| Kurtosis | 0.168 | −0.108 | 0.307 | −0.066 | −0.693 | −0.163 |
| | Direct Drilling | | | | | |
| Mean | 24.04 | 23.54 | 23.35 | 55.97 | 56.82 | 60.27 |
| SE | 0.19 | 0.17 | 0.18 | 0.53 | 0.74 | 0.53 |
| Median | 23.96 | 23.57 | 23.38 | 56.19 | 55.82 | 60.64 |
| Min. | 22.60 | 21.94 | 21.51 | 48.86 | 50.98 | 53.40 |
| Max. | 25.62 | 25.24 | 25.11 | 60.18 | 63.93 | 64.89 |
| SD | 0.99 | 0.89 | 0.93 | 2.77 | 3.82 | 2.77 |
| CV | 0.041 | 0.038 | 0.040 | 0.049 | 0.067 | 0.046 |
| Skewness | 0.054 | −0.179 | −0.249 | −0.748 | 0.294 | −0.458 |
| Kurtosis | −1.43 | −0.731 | −0.305 | 0.272 | −0.949 | 0.206 |
| | Total | | | | | |
| Mean | 23.49 | 23.20 | 23.11 | 55.53 | 56.92 | 60.05 |
| SE | 0.15 | 0.13 | 0.13 | 0.37 | 0.51 | 0.38 |
| Median | 23.34 | 23.11 | 23.18 | 55.88 | 57.09 | 60.50 |
| Min. | 20.71 | 21.42 | 21.20 | 48.86 | 49.49 | 53.21 |
| Max. | 25.62 | 25.24 | 25.11 | 60.18 | 64.33 | 64.89 |
| SD | 1.09 | 0.93 | 0.95 | 2.73 | 3.72 | 2.79 |
| CV | 0.046 | 0.040 | 0.041 | 0.049 | 0.065 | 0.047 |
| Skewness | 0.055 | 0.107 | −0.033 | −0.534 | 0.104 | −0.608 |
| Kurtosis | −0.346 | −0.741 | −0.295 | −0.13 | −0.886 | −0.039 |

## Soil Water Content Measurement

Between January 2008 and March 2009, three of the CT and DD plots were sampled on 26 d for gravimetric soil water content ($\theta_g$). During each survey, 54 soil samples were taken at depths of 0 to 0.10 and 0.25 to 0.35 m (Fig. 1A). The soil samples were weighed and dried at 105°C for 48 h. The $\theta_g$ of the top 0.35 m was calculated as a weighted average of the 0- to 0.10- and 0.25- to 0.35-m $\theta_g$ using weighting factors of 0.33 and 0.66, respectively. Volumetric θ was also monitored in Plots CT1 and DD1 (Fig. 1A) using four Enviroscan multisensor capacitance probes (Sentek Sensor Technologies, Stepney, SA, Australia) with sensors at 0.10-, 0.20-, 0.30-, 0.60-, and 0.90-m depths. A site-specific calibration was available to convert the scaled frequency (SF) measured by this sensor. Using a Diviner 2000 single-sensor capacitance probe (Sentek Sensor Technologies), the SF was also periodically measured up to the 1-m depth, in 0.10-m increments, in the three CT and DD plots at 18 equally distributed locations. For this sensor, no site-specific calibration of the θ–SF relation was available, so results are reported as SF.

## Soil Apparent Electrical Conductivity Measurement

The field was surveyed on 13 dates between March 2006 and 2009, between harvest and sowing, according to tillage and for different soil moisture conditions. The $EC_a$ was measured using a noninvasive, electromagnetic induction sensor (EM38-DD, Geonics, Mississauga, ON, Canada), which consists of two superposed EM38 sensors, one in the horizontal and the other in the vertical dipole mode, providing shallow ($EC_{as}$) and deep ($EC_{ad}$) measurements, respectively. The cumulative response of the EM38, as proposed by Callegary et al. (2007), is a function of both soil $EC_a$ and the coil orientations. The present case can be simplified using a two-layer model with $EC_a$ values of 50 and 100 mS $m^{-1}$ for the topsoil and subsoil layers, respectively, leading to effective exploration depths 0.6 and 0.9 m for the horizontal and vertical dipoles, respectively (Callegary et al., 2007). Before soil sensing, the instrument was zeroed at 1.5 m above the soil surface, as recommended by the manufacturer. This operation was repeated before each survey in the same area of the field. The sensor was hosted in an isolated polyvinyl chloride sled and pulled by an all-terrain vehicle equipped with a real-time kinematic differential global positioning system receiver, a guidance bar for parallel swathing at 3 m, and a field computer to log the $EC_a$ data and three-dimensional coordinates with a frequency of 1 Hz. Soil sensing was performed perpendicular to the principal orientation of the plots. At the end of each survey, $EC_a$ was measured along a diagonal transect to check for sensor drift <5% of the mean $EC_{as}$ and $EC_{ad}$. The dates of the $EC_a$ surveys and soil surface state are detailed in Table 2.

Table 2. Sampling dates, crops in rotation, and soil conditions for each apparent electrical conductivity survey.

| Survey | Case | Date | Measurements | Crop in rotation | Soil surface conditions |
|---|---|---|---|---|---|
| | | | no. | | |
| 1 | B | 10 Mar. 2006 | 7201 | sunflower | fallow |
| 2 | B | 29 Mar. 2006 | 5624 | sunflower | fallow |
| 3 | | 3 Oct. 2006 | 5085 | field pea | fallow |
| 4 | | 15 Nov. 2006 | 1664 | field pea | fallow |
| 5 | | 20 Sept. 2007 | 1324 | wheat | field pea residue |
| 6 | | 10 Oct. 2007 | 3009 | wheat | field pea residue |
| 7 | C | 7 Nov. 2007 | 5612 | wheat | field pea residue |
| 8 | C | 29 Nov. 2007 | 5449 | wheat | field pea residue |
| 9 | | 18 Aug. 2008 | 4660 | wheat | wheat residue |
| 10 | A | 18 Sept. 2008 | 4655 | sunflower | wheat residue |
| 11 | A | 10 Nov. 2008 | 6200 | sunflower | fallow |
| 12 | D | 20 Nov. 2008 | 4899 | sunflower | fallow |
| 13 | D | 18 Feb. 2009 | 6737 | sunflower | fallow |

## Data Analysis

Point $EC_a$ measurements were interpolated using ordinary kriging with local variogram calculation (Minasny et al., 2005). The interpolated data were used for further analysis.

Relative differences for $\theta_g$ ($\delta\theta_{ij}$) and $EC_a$ ($\delta EC_{as,ij}$ and $\delta EC_{ad,ij}$) were calculated according to Vachaud et al. (1985):

$$\delta Z_{ij} = \frac{Z_{ij} - \langle Z \rangle_j}{\langle Z \rangle_j} \qquad [1]$$

where $Z_{ij}$ is the $\theta_g$ or $EC_a$ at the $i$th location and $j$th survey time and $\langle Z \rangle_j$ is the spatial average of the field at the $j$th survey time. Relative differences allowed the standardization of $\theta_g$ and $EC_a$ values for each survey, reducing the effect of different soil and weather conditions and providing a way to identify areas where $\theta_g$ and $EC_a$ values were higher, lower, or close to their spatial means. Relative differences also allowed the non-absolute $EC_a$ values measured with the EM38DD to be dealt with, because its calibration is specific for the governing soil conditions during each survey. For each $i$th location, the mean relative difference ($Z$–$MRD_i$) and the corresponding standard deviation of the 13 $EC_a$ surveys and the 26 $\theta_g$ campaigns were calculated and plotted to evaluate the temporal persistence or rank stability of their spatial patterns:

$$Z\text{-MRD}_i = \frac{1}{N}\sum_{j=1}^{s} \delta Z_{ij} \qquad [2]$$

where $s$ is the total number of surveys. Locations representing the spatial mean in all the surveys will give $Z$–MRD values close to zero. Interpolation by ordinary kriging of $\theta_g$–MRD was done with SGeMS (Remy et al., 2009) using a spherical variogram model.

Principal component analysis was performed (Davis, 2002) using $\delta EC_{as,ij}$ and $\delta EC_{ad,ij}$ ($\delta EC_a$ hereafter) data from the 13 surveys to identify the main common underlying sources of variability and to group similar surveys. The PCA scores corresponding to the first three PCs were mapped and associated with physical attributes of the field. Only the first three PCs were retained because the fourth PC explained a smaller part of the total variance than each survey separately. To elucidate changing soil conditions caused by transient properties such as θ or porosity, we used maps of $\delta EC_a$ increments, calculated as the difference between successive $\delta EC_a$ surveys (Martínez et al., 2009; Robinson et al., 2009). To illustrate this, we considered four cases (A–D) covering a wide range of soil conditions.

Case A (Surveys 10 and 11) corresponded to a fallow period in autumn 2008, after wheat was harvested. During the period between both $EC_a$ surveys, a herbicide was applied over all the field and the CT and MT plots were tilled on 6 October with a moldboard plow and a disk harrow, respectively. The period had

19 rainfall events, of which one of them (30 mm $d^{-1}$) represented three-fourths of the total rainfall.

Case B (Surveys 1 and 2) corresponded to another fallow period after wheat in spring 2006. The CT and MT plots were plowed and disked, respectively, during the fall while during the winter, the CT and MT plots were tilled with a cultivator. During the period between the two $EC_a$ surveys, the CT and MT plots were tilled with a chisel plow. The DD plots remained undisturbed after wheat harvest until sunflower drilling in April 2006. The total rainfall during this period was 66 mm, distributed in six events, with a maximum intensity of 26 mm $d^{-1}$ 9 d before Survey 2.

In Case C, transformed $EC_a$ data from Surveys 7 and 8 were used. The field was left fallow after field pea in autumn 2007 and an intense rainfall event of 115 mm $d^{-1}$ occurred on 20 Nov. 2007.

Case D shows the differences between Surveys 12 and 13, during the winter of 2008 to 2009, when the soil was left fallow after the wheat harvest. The soil was tilled with a moldboard plow in the CT system and a disk harrow in the MT system during fall 2008. The total rainfall during the period between the two surveys was 197 mm as a result of several low- to medium-intensity rainfall events.

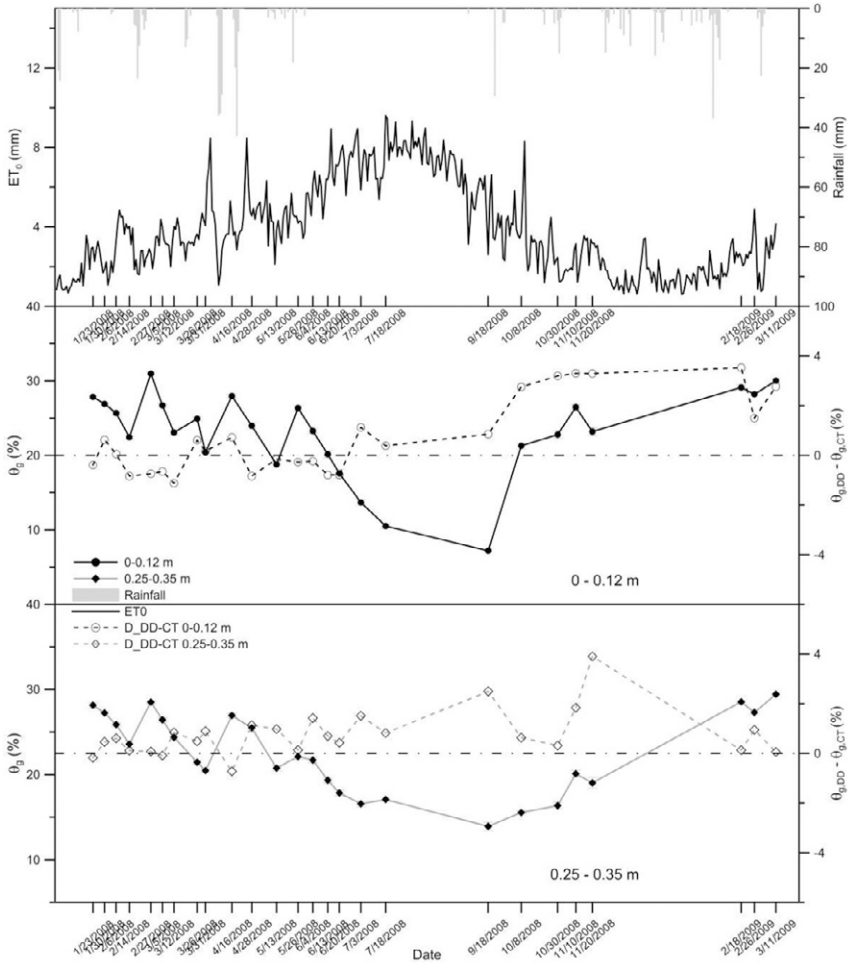


Fig. 2. Daily rainfall and reference evapotranspiration, $ET_0$ (top), gravimetric soil moisture content ($\theta_g$) in the 0- to 0.12- and 0.25- to 0.35-m depths during the period 1 Jan. 2008 to 15 Mar. 2009, and the difference in $\theta_g$ between direct drilling (DD) and conventional tillage (CT) sampling locations (middle and bottom).

# Results and Discussion

## Soil Water Content Dynamics

Between January 2008 and March 2009, excluding the summer period (June–September 2008), $\theta_g$ ranged from 0.20 to 0.30 kg $kg^{-1}$, with an average of 0.23 kg $kg^{-1}$ for both the topsoil (0–0.10 m) and the subsoil (0.25–0.35 m). During summer, the soil water content decreased below 0.20 kg $kg^{-1}$ in the subsoil and below 0.10 kg $kg^{-1}$ in the topsoil, with soil cracks starting to develop. During the first wet season, January to April 2008, the subsoil and topsoil $\theta_g$ values were similar (Fig. 2). As the soil dried, differences between depths increased, reaching a maximum by the end of the summer. The dry topsoil, covered by a crust, contributed efficiently to water conservation in the subsoil. Also, the topsoil $\theta_g$ was more sensitive to rainfall and evaporation. As a consequence, $\theta$ variations in the subsoil were smaller than those found in the topsoil, in accordance with the force–restore theory of Deardorff (1977). After the summer, differences between depths tended to disappear and a situation similar to that of winter 2008 was achieved. Gravimetric soil water content was generally higher under DD than CT. The maximum range of $\theta_g$, 0.14 $m^3$ $m^{-3}$, occurred on 28 Apr. 2008 and 18 Feb. 2009 for the top- and subsoil, respectively, and was smaller than the $\theta$ ranges found in the works of Kachanoski et al. (1988) and McCutcheon et al. (2006) (0.30 and 0.23 $m^3$ $m^{-3}$, respectively).

## Temporal Stability Analysis of Soil Water Content

Generally, for each sampling depth, locations representing the spatial mean in all the surveys (dashed line in Fig. 3, where $\theta_g$–MRD = 0) differed. Only Location 27 showed a $\theta_g$–MRD value close to zero for all sampling depths, indicating that it would be a good location for measuring the spatial mean $\theta$ throughout the soil profile on each sampling date. The topsoil had the largest number of candidates with $\theta_g$–MRD near zero. These locations corresponded to Locations 2, 49, 50, 3, 11, 43, 52, 44, 6, and 8. The mean relative difference for the 0.25- to 0.35-m horizon ranged from −0.004 to 0.004 at Locations 7, 27, 13, 30, 33, and 53 and for the 0- to 0.35-m horizon at Locations 8 and 27. Locations with $\theta_g$–MRD values close to zero were associated with intermediate

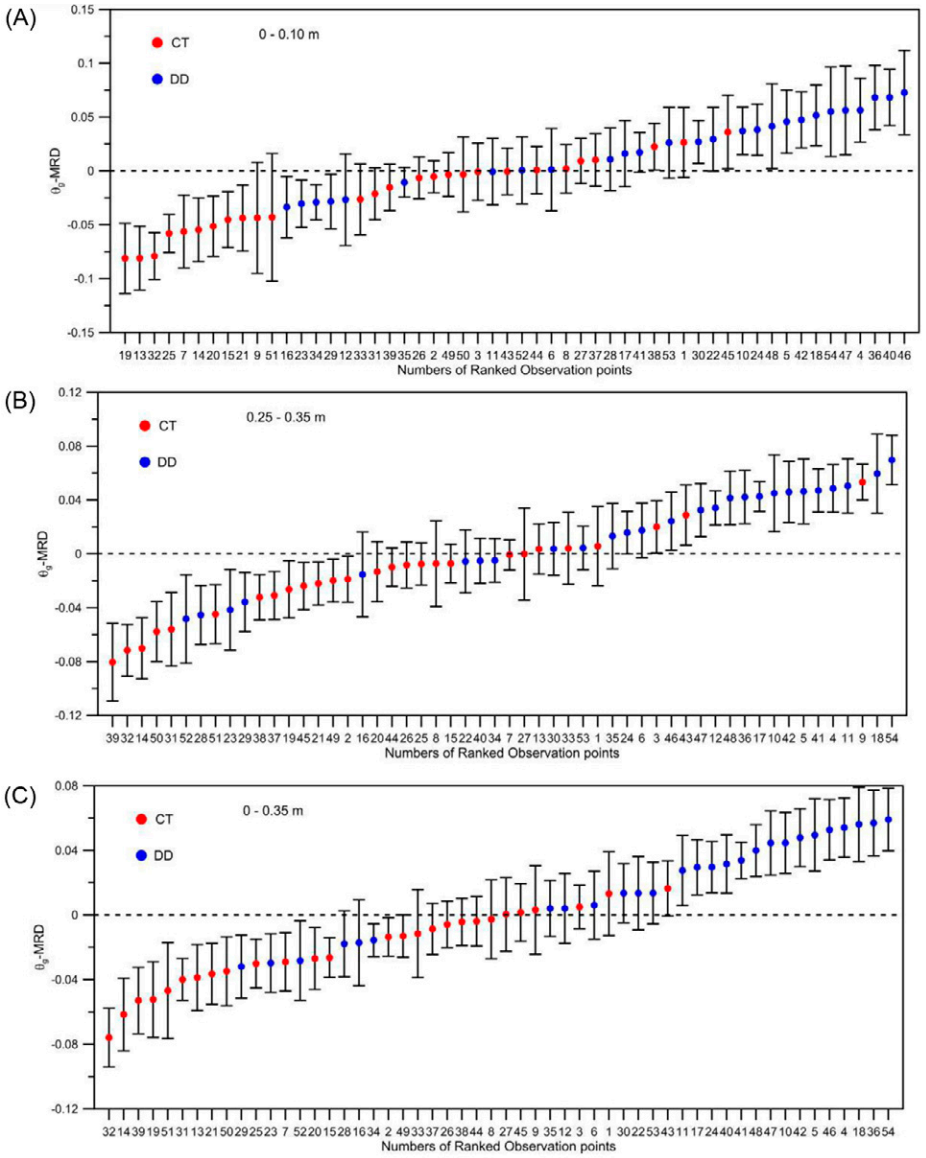


Fig. 3. Rank stability plots of gravimetric soil water content mean relative differences ($\theta_g$–MRD) for conventional tillage (CT) and direct drilling (DD) sampling locations, obtained from 26 gravimetric surveys, for the (A) 0- to 0.10-, (B) 0.25- to 0.35-, and (C) 0- to 0.35-m depths.

topographic attributes (Grayson and Western, 1998; Gomez-Plaza et al., 2000). For the topsoil layer, Locations 19, 13, and 32 were persistently drier, while for the 0.25- to 0.35- and 0- to 0.35-m depths, Locations 39, 32, and 14 were the driest locations, indicating the dominant effect of the subsoil on the temporal stability for the considered soil depth. As a result, Location 32 could be considered as the persistently driest location of the field. This location was within a CT plot, close to the main water divide and had a medium to high slope (3°). The persistently wettest locations varied more among the different depths, as also observed by Tallon and Si (2003), although a significant correlation of 0.52 ($P < 0.05$) was found between the $\theta_g$–MRD of the 0- to 0.10- and 0.25- to 0.35-m depths. Locations 36, 40, and 46 were the wettest for the 0- to 0.10-m depth, Locations 18 and 54 for the 0.25- to 0.35-m depth, and Locations 18, 36, and 54 for the 0- to 0.35-m depth, showing again the different behavior of the topsoil. Locations 18, 36, and 54 were situated in the lowest area of the field and were considered as the wettest spots. Generally, the spatial patterns of $\theta_g$–MRD were related to tillage and topography, as shown in Fig. 4. Lower $\theta_g$–MRD values were found within the CT plots, especially in the highest part of the field, near the water divide, while the DD plots, especially in the lowest areas, showed the highest $\theta_g$–MRD. The different behavior of top- and subsoil (Fig. 4A and 4B) has important consequences in hydrologic applications for θ monitoring and modeling using topsoil θ remote sensing (Manfreda et al., 2007).

## Spatial and Temporal Variability of Apparent Electrical Conductivity

The spatial mean $EC_{as}$ and $EC_{ad}$ for the 13 surveys ranged from 27 to 84 and from 80 to 137 mS $m^{-1}$, with mean values of 59 and 104 mS $m^{-1}$, respectively. The extreme values for $EC_{as}$ and $EC_{ad}$ were observed on different days, indicating different topsoil and subsoil dynamics. In general, higher $EC_a$ values were observed during wet periods (e.g., Nadler, 2005), while the lowest values were found during dry periods, after the summer season and harvest time (Fig. 5). Changes in the spatial mean $EC_{as}$ were higher than those of $EC_{ad}$ because the main causes of temporal variability such as drying–wetting (and shrinkage–swelling), tillage, and root development occur mainly in the topsoil. In general, probability density functions of both $EC_{as}$ and $EC_{ad}$ were close to normal or slightly positively skewed as a consequence of high $EC_a$ values in the lowest part of the field, where water and sediments accumulated as a result of surface and subsurface flow.

## Principal Component Analysis of Spatiotemporal Apparent Electrical Conductivity Data

The first three PCs represented about 90% of the total variance. For $\delta EC_{as}$, they accounted for 65, 14, and 11% and for $\delta EC_{ad}$, 74, 13, and 6% of the total variance, respectively. The mean $\delta EC_{as}$ and $\delta EC_{ad}$ values had correlation coefficients of −0.995 and −0.998 with PC1, indicating that this PC represents the combination of time-invariable properties (particle size, shape, and orientation,

cation exchange capacity, wettability, soil effective depth) leading to the average $EC_a$ patterns of the field. Figure 6 shows the circles of correlation with the 13 $\delta EC_{as}$ surveys projected on the planes defined by the first three PCs. The coordinates represent the correlation coefficients between the $\delta EC_{as}$ for each survey and the PCs. The highest correlation between PC1 and $\delta EC_{as}$ and $\delta EC_{ad}$, −0.4, was found for Survey 4. This indicates that for the expansive clay soil of this study, which is characterized by a large temporal variability in soil physical properties, a single survey is far from sufficient to obtain the average $EC_a$–related field pattern. In contrast to Johnson et al. (2003) and Farahani and Buchleiter (2004), who worked with coarser soils with a higher degree of temporal stability in soil physical properties and $EC_a$, the fine-textured soil of the Tomejil Farm needs at least several surveys to capture a time-stable pattern.

According to PC1 and PC2, the 13 surveys could be separated into four groups. A first group, including Surveys 10, 11, and 12, covered the 2008 fall period before sunflower sowing. A second group consisted of Surveys 5, 6, and 7, which took place during fall 2007 before wheat sowing and before an intense rainfall event on 20 Nov. 2007, which sharply increased the soil moisture content and contributed to rill development in the MT and CT plots. A rather heterogeneous group was formed by Surveys 1, 3, and 4, with low and similar contributions to PC1 and PC2, covering a broad range of soil conditions. Surveys 8, 9, and 13 were rather singular, showing large differences with respect to the other surveys. Survey 8 took place after an intense rainfall event, Survey 9 during the summer after wheat harvest, and Survey 13 after a long rainy period.

## Spatial Patterns of Principal Component Analysis Scores

As expected, the pattern of the PC1 scores (Fig. 7A), which explained the largest part of the total variability of

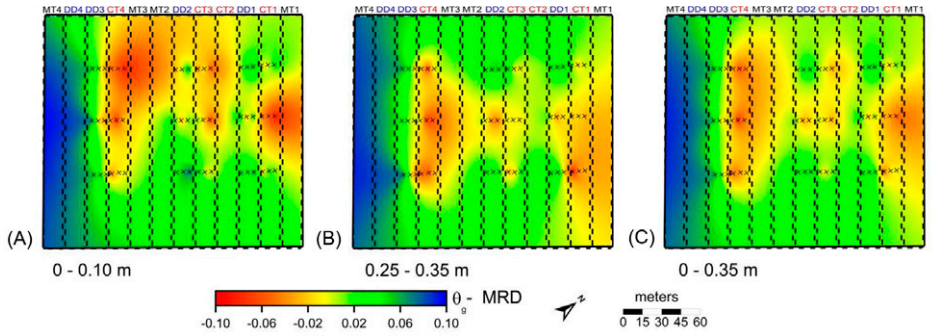


Fig. 4. Ordinary kriging maps of gravimetric soil water content mean relative difference ($\theta_g$ MRD) for the (A) 0- to 0.10-, (B) 0.25- to 0.35-, and (C) 0- to 0.35-m horizons. Gravimetric sampling locations are indicated by X.

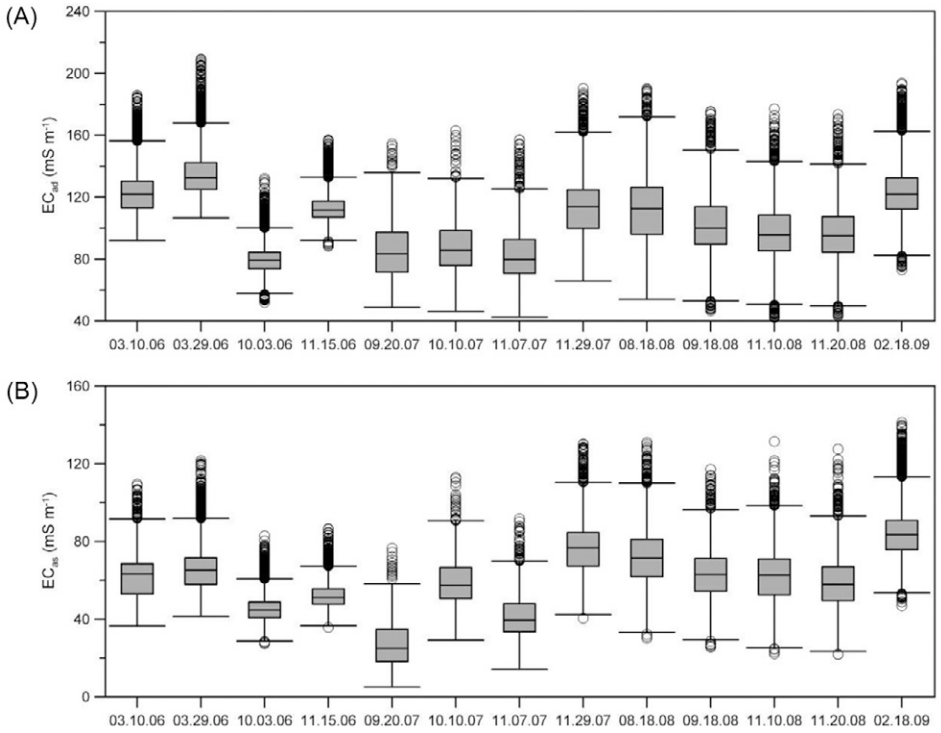


Fig. 5. Box and whisker plots for (A) deep ($EC_{ad}$) and (B) shallow apparent electrical conductivity ($EC_{as}$) from 13 surveys from 10 Mar. 2006 to 18 Feb. 2009. Circles represent values outside the 95% confidence interval, whiskers indicate maximum and minimum values at the 95% confidence level, the top and the bottom of the box show the 25th and 75th percentiles, and the line inside the box is the median value.

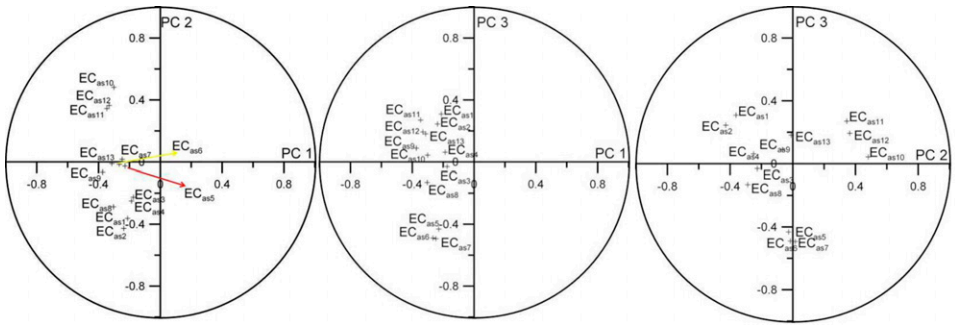


Fig. 6. Circles of correlation, showing the projections of the 13 shallow apparent electrical conductivity ($EC_{as}$) surveys on the planes defined by the first three principal components (PCs).

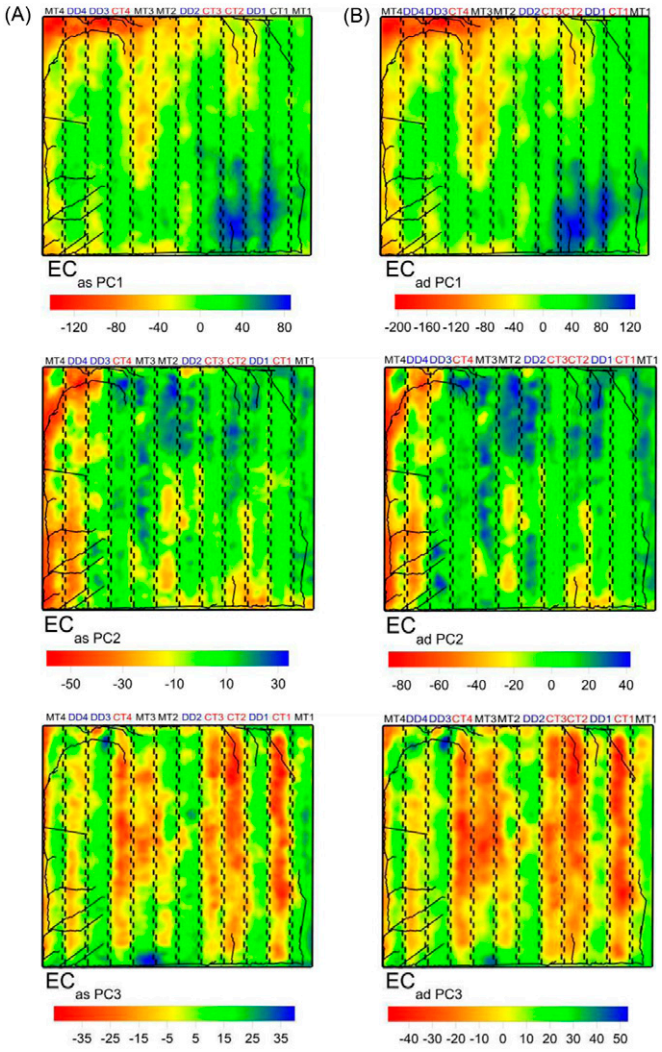


Fig. 7. Maps of the scores of the first three principal components for (A) deep ($EC_{ad}$) and (B) shallow apparent electrical conductivity ($EC_{as}$) (MT, minimum tillage; DD, direct drilling; CT, conventional tillage).

the spatiotemporal data set, was similar to the mean $\delta EC_a$ pattern. Significant ($P < 0.001$) correlation coefficients were found between $\delta EC_a$ and the PC1 scores. Therefore, PC1 was associated with the underlying patterns of time-invariant soil properties that contributed most to the mean $\delta EC_a$ pattern. The pattern of the second component could be roughly related with topographic attributes such as slope and aspect, while PC3 showed a pattern related to soil management. The spatial patterns of the PC1 and PC2 scores had in common features linked to soil-water dynamics related to drainage networks (Fig. 1B and 7). Because these PCs accounted for most of the $\delta EC_{as}$ and $\delta EC_{ad}$ variability, soil water dynamics and topography could be considered major sources of $\delta EC_a$ variability. High $\delta EC_a$ or low PC1 scores were mainly located in the lowest areas of the field, especially on the northwest border of MT4 to CT4 and along MT4. This area received most of the runoff water and sediments not only from this field but also from an adjacent field. Drainage lines on the northwest edge of DD1 to CT2 and CT2 to CT3 were also associated to low PC1 scores (high $\delta EC_a$). Drainage lines located in the southeast part of MT1 and CT2 did not accumulate much water and sediments because they had a smaller contributing area, with a deeper soil, where slickensides at 0.3-m depth were frequent, as visually observed during soil sampling. Moreover, the field was unbounded at its eastern and southern edges, preventing water from accumulating. The spatial pattern of PC2 showed topographic and hydromorphic features that mainly appeared in the southern part of the field. During the first decade of the soil management experiment, this area was often flooded until a ditch was dug to evacuate excess water. Soil management effects could be linked to PC3 because a band-type pattern occurs in the principal direction of the tillage subplots (Fig. 7), where bands with low PC3 scores mainly appeared in the CT plots. Lower PC3 scores were also found in parts of the MT3 and MT4 plots.

## Tillage and Soil Moisture Effects on Apparent Electrical Conductivity

Maps of $\delta EC_{as}$ and $\delta EC_{ad}$ increments for Surveys 10 and 11 (Case A, Fig. 8A) and Surveys 1 and 2 (Case B, Fig. 9A) show the effects of both tillage and changing soil physical properties on $EC_a$. In Case A, the rainfall events increased the soil moisture in the top 0.3-m depth (Fig. 8C). The largest $\delta EC_a$ negative increments were found in the CT plots, while DD and MT plots showed generally positive increments or small negative differences. This fact could be a consequence of a greater increase in topsoil porosity in the CT plots after moldboard plowing. This resulted in similar $\delta EC_{as}$ and $\delta EC_{ad}$ increment patterns but with a smaller decrease in CT for the latter due to a deeper effective exploration. As a consequence, in this case, $EC_a$ values varied between the two surveys as a result of changing topsoil properties due to tillage. In Case B (Fig. 9A), the CT plots showed the highest $\delta EC_a$ increments associated with their greater porosity after tillage (Hewitt and Dexter, 1980; Or and Ghezzehei, 2002), which contributed to a larger pore volume available for water filling. Direct-drill plots had a larger proportion of their pores filled by water and had a lower volume available for water filling. In addition, because the DD plots had already higher $EC_a$ values before rainfall, their $\delta EC_a$ increments were proportionally smaller than those of the CT and MT plots. Minimum tillage plots showed an intermediate behavior between CT and DD. Tillage effects were clearer in the $\delta EC_{as}$ difference maps because this operation influenced soil physical properties within the top 0.2 m.

Cases C and D (Fig. 10A and 11A) illustrate the hydrologic response of the field to an intense shower and to a long wet period with several low- to medium-intensity rainfall events, respectively. In Case C, the largest $\delta EC_{as}$ and $\delta EC_{ad}$ increments occurred in the DD plots as a consequence of larger $\theta$ increments. The pattern of the $\delta EC_{as}$ increments showed a significant correlation of 0.57 ($P < 0.01$) with the $\theta_g$–MRD (0–0.35 m) pattern (Fig. 12A). Both $\theta_g$–MRD and $\delta EC_{as}$ increment patterns could be explained as

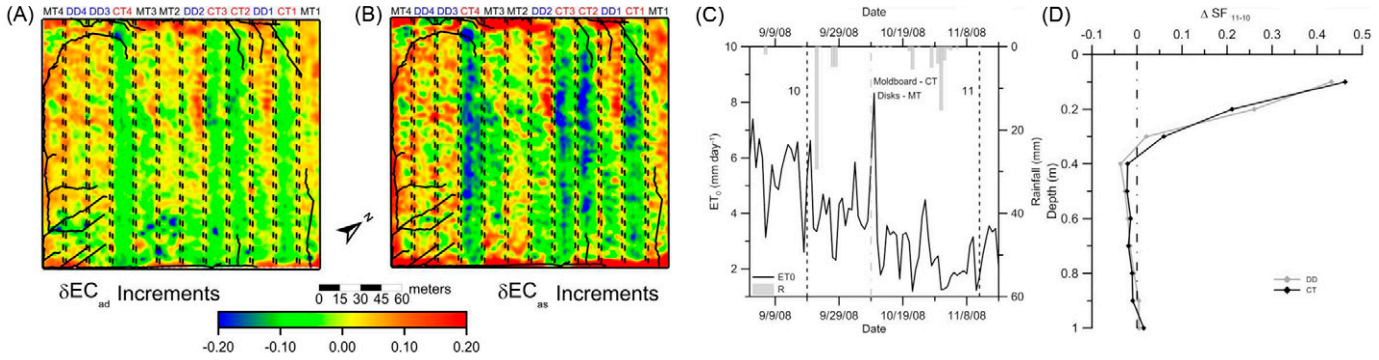


Fig. 8. Increments of the apparent electrical conductivity ($EC_a$) relative difference in (A) shallow ($\delta EC_{as}$) and (B) deep $EC_a$ ($\delta EC_{ad}$) between Surveys 10 and 11 (Case A), showing the effect of soil tillage on $EC_a$; (C) daily rainfall, evapotranspiration ($ET_0$), and tillage type and date for the period of the two $EC_a$ surveys from September to November 2008; and (D) increments of scaled frequency ($\Delta SF$) obtained with the Diviner single-sensor capacitance probe, as a proxy for soil water content increments, under conventional tillage (CT) and direct drilling (DD).

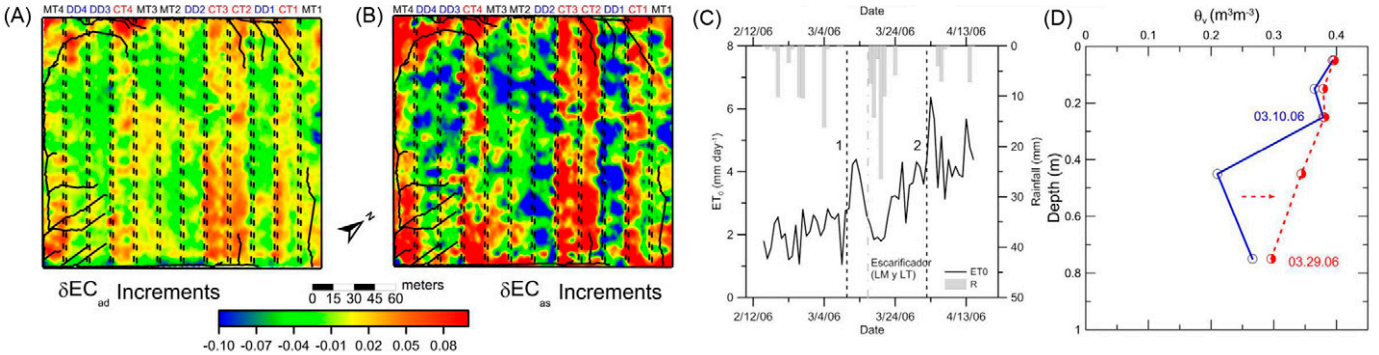


Fig. 9. Increments of the apparent electrical conductivity ($EC_a$) relative difference in (A) shallow ($\delta EC_{as}$) and (B) deep $EC_a$ ($\delta EC_{ad}$) between Surveys 1 and 2 (Case B), showing the mixed effect of soil tillage and rainfall on $EC_a$; (C) daily rainfall, evapotranspiration ($ET_0$), and tillage type and date for the period of the two $EC_a$ surveys from February to April 2006; and (D) volumetric soil water content ($\theta_v$) obtained with the Enviroscan multisensory capacitance probes under conventional tillage (CT) and direct drilling (DD).

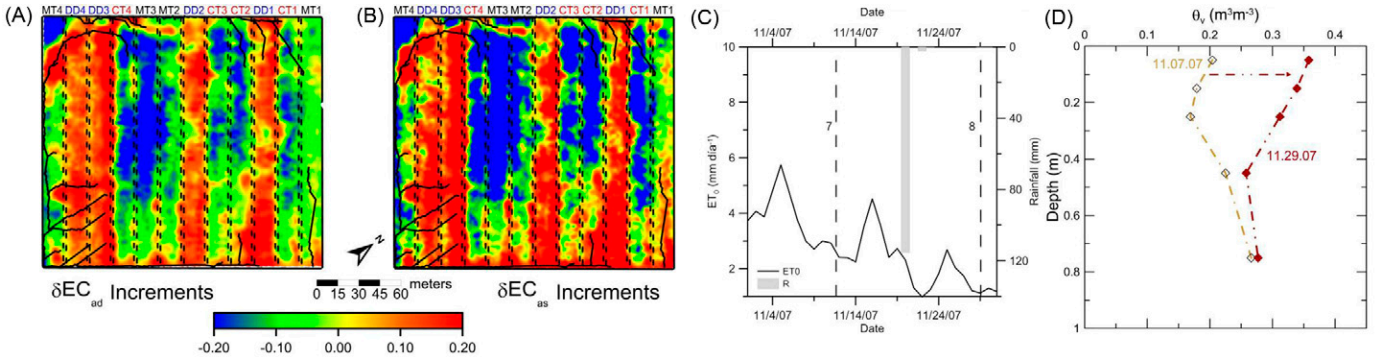


Fig. 10. Increments of the apparent electrical conductivity ($EC_a$) relative difference in (A) shallow ($\delta EC_{as}$) and (B) deep $EC_a$ ($\delta EC_{ad}$) between Surveys 7 and 8 (Case C), showing the effect of an intense rainfall event on $EC_a$; (C) daily rainfall, evapotranspiration ($ET_0$), and tillage type and date for the period of the two $EC_a$ surveys in November 2007; and (D) volumetric soil water content ($\theta_v$) obtained with the Enviroscan multisensory capacitance probes under conventional tillage (CT) and direct drilling (DD).

functions of the topographic and soil management features of the field, with, in general, negative increments of $\delta EC_{as}$ and $\theta_g$–MRD within the CT plots and in the highest part of the field near the water divide. Positive $\delta EC_{as}$ increments and $\theta_g$–MRD values were common within the DD plots and especially in the lowest part of the field and along a part of the drainage network. Negative $\delta EC_{as}$, generally found in the CT and MT plots, could be associated with proportionally lower θ increments under these treatments in comparison to DD plots. Case D (Fig. 11A), in contrast to Case C, does not show clear effects of soil management on the $\delta EC_{as}$ and

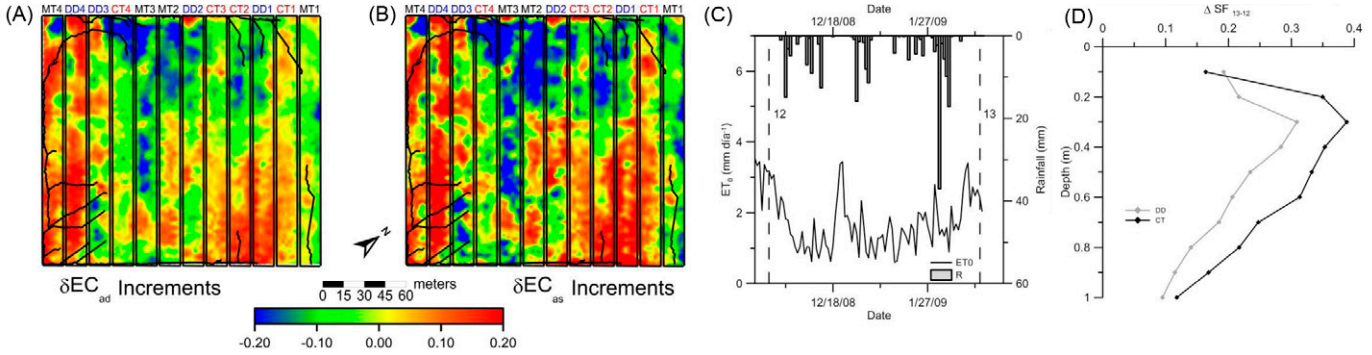


Fig. 11. Increments of the apparent electrical conductivity ($EC_a$) relative difference in (A) shallow ($\delta EC_{as}$) and (B) deep $EC_a$ ($\delta EC_{ad}$) between Surveys 12 and 13 (Case D), showing the effect of a prolonged wet period on $EC_a$; (C) daily rainfall, evapotranspiration ($ET_0$), and tillage type and date for the period of the two $EC_a$ surveys on 18 Dec. 2008 and 27 Jan. 2009; and (D) increments of scaled frequency ($\Delta SF$) obtained with the Diviner single-sensor capacitance probe, as a proxy for soil water content increments, under conventional tillage (CT) and direct drilling (DD).

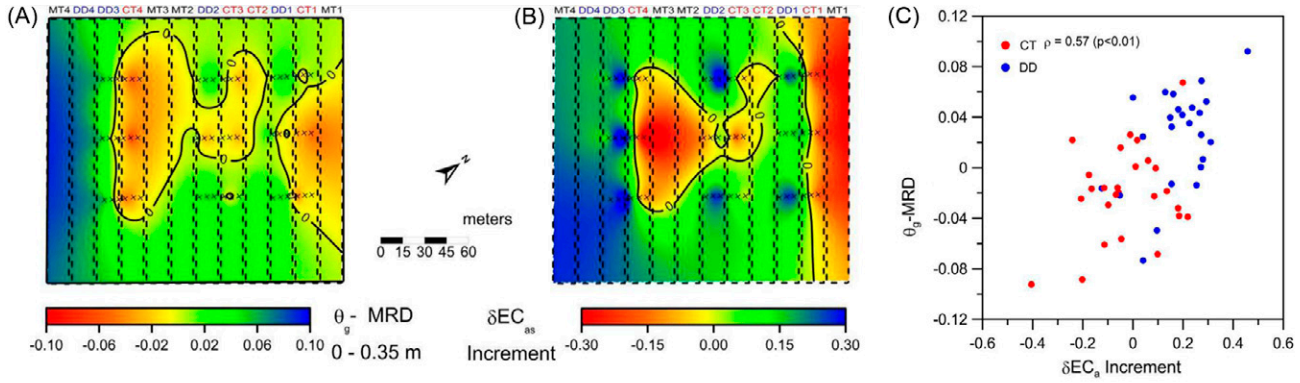


Fig. 12. (A) Spatial patterns of the mean relative differences of gravimetric soil water content ($\theta_g$–MRD) for the 0- to 0.35-m depth calculated from 26 $\theta_g$ surveys, (B) the increments of the shallow apparent electrical conductivity relative differences ($\delta EC_{as}$) between Surveys 7 and 8 as interpolated from the 54 measurement locations where soil sampling took place, and (C) the relationship between $\theta_g$–MRD and $\delta EC_{as}$ increments between Surveys 7 and 8.

$\delta EC_{ad}$ increments. For this case, the $\delta EC_{as}$ and $\delta EC_{ad}$ increment patterns were related rather to slope and aspect as a result of horizontal redistribution of soil moisture as a function of topography. Areas with high $\delta EC_{as}$ and $\delta EC_{ad}$ increments where located in the south orientation area of the field, which generally has low $EC_a$ and consequently has a proportionally higher increment in $\delta EC_a$ than other areas of the field, and in the flat area in MT4 to DD4 where most of the water accumulates.

## Conclusions

The usefulness of a framework for $EC_a$–based field-scale soil pattern characterization was illustrated using a sequence of 13 $EC_{as}$ and $EC_{ad}$ surveys of the same field. Top- and subsoil were explored independently by the sensor and differences between them could be related to varying soil properties with depth. Larger $EC_a$ values, a smaller variability, and different dates for minimum and maximum $EC_a$ as related to different soil moisture conditions were found in the subsoil compared with the topsoil. Differences between the two soil horizons were also found for θ, which became larger as the soil dried and smaller as it was wetted. The time-stable, mean pattern for the $EC_{as}$ and $EC_{ad}$ surveys were related to topographic characteristics, soil depth, and soil structure. Principal component analysis was used to detect the main sources of variation from the $EC_{as}$ and $EC_{ad}$ data sets. The first three components accounted for 90% of the $EC_{as}$ and $EC_{ad}$ variability and were related to soil spatial variability, soil management, and topography. Following the PCA, the $EC_a$ surveys could be grouped according to similar soil conditions or exceptional situations (i.e., intense rainfall, a long rainy period, and summer surveys). The spatial patterns of the first three PC scores highlighted patterns caused mainly by topography and associated water dynamics, with areas of high $EC_a$ situated in the lowest part of the field, along the drainage network, and in the CT plots, as expressed by a band-type pattern in the field. The temporal $EC_a$ data set also allowed determination that, for a fine-textured soil where the soil physical properties can change with time, the mean spatial pattern was different from the individual patterns identified on each survey. Patterns of changing soil conditions, as a result of a variation in porosity or θ, were successfully elucidated by comparing $EC_a$ data from successive surveys, and

showed the effects of tillage and external forcing at the field scale. The electromagnetic induction sensing system used in this study was found to be very adequate for mapping changes in $EC_a$–related time-variable soil properties such as soil water content and could therefore be used to compare the spatially distributed performance of different soil management systems at the field scale in uniform clay soil that exhibits small spatial soil water content ranges.


## Acknowledgments

This work was funded by INIA and FEDER through Grants RTA2006-00058-CO3-02 and PRE-2005, by the Junta de Andalucía though the Grants AGR-2349 and AGR-4782, and by the Ministry of Science and Innovation and FEDER through Grant AGL2009-12936-C03-03. We thank the staff of the Soil and Water Group at IFAPA Las Torres-Tomejil for their assistance with the field sampling and soil analysis. Also special thanks to J. Osuna (University of Cordoba) and M. Morón (IFAPA) for setting up the mobile $EC_a$ measurement system.


# References


Abdu, H., D.A. Robinson, M. Seyfried, and S.B. Jones. 2008. Geophysical imaging of watershed subsurface patterns and prediction of soil texture and water holding capacity. Water Resour. Res. 44:W00D18, doi:10.1029/2008WR007043.

Bogena, H.R., J.A. Huisman, H. Meier, U. Rosenbaum, and A. Weuthen. 2009. Hybrid wireless underground sensor networks: Quantification of signal attenuation in soil. Vadose Zone J. 8:755–761.

Callegary, J.B., T.P.A. Ferré, and R.W. Groom. 2007. Vertical spatial sensitivity and exploration depth of low-induction-number electromagnetic-induction instruments. Vadose Zone J. 6:158–167.

Davis, J.C. 2002. Statistics and data analysis in geology. 3rd ed. John Wiley & Sons, New York.

Deardorff, J.W. 1977. A parameterization of ground-surface moisture content for use in atmospheric prediction models. J. Appl. Meteorol. 16:1182–1185.

Evett, S.R., and G.W. Parkin. 2005. Advances in soil water content sensing: The continuing maturation of technology and theory. Vadose Zone J. 4:986–991.

Farahani, H.J., and G.W. Buchleiter. 2004. Temporal stability of soil electrical conductivity in irrigated sandy fields in Colorado. Trans. ASAE 47:79–90.

Friedman, S.P. 2005. Soil properties influencing apparent electrical conductivity: A review. Comput. Electron. Agric. 46:45–70.

Gomez-Plaza, A., J. Alvarez-Rogel, J. Albaladejo, and V.M. Castillo. 2000. Spatial patterns and temporal stability of soil moisture across a range of scales in a semi-arid environment. Hydrol. Processes 14:1261–1277.

Grayson, R.B., and A.W. Western. 1998. Towards areal estimation of soil water content from point measurements: Time and space stability of mean response. J. Hydrol. 207:68–82.

Guber, A.K., T.J. Gish, Y.A. Pachepsky, M.Th. van Genuchten, C.S.T. Daughtry, T.J. Nicholson, and R.E. Cady. 2008. Temporal stability in soil water content patterns across agricultural fields. Catena 73:125–133.

Hewitt, J.S., and A.R. Dexter. 1980. Effects of tillage and stubble management on the structure of a swelling soil. Eur. J. Soil Sci. 31:203–215.

Johnson, C.K., D.A. Mortensen, B.J. Wienhold, J.F. Shanahan, and J.W. Doran. 2003. Site-specific management zones based on soil electrical conductivity in a semiarid cropping system. Agron. J. 95:303–315.

Kachanoski, R.G., E.G. Gregorich, and I.J. van Wesenbeeck. 1988. Estimating spatial variations of soil-water content using noncontacting electromagnetic inductive methods. Can. J. Soil Sci. 68:715–722.

Lambot, S., L. Weihermüller, J.A. Huisman, H. Vereecken, M. Vanclooster, and E.C. Slob. 2006. Analysis of air-launched ground-penetrating radar techniques to measure the soil surface water content. Water Resour. Res. 42:W11403, doi:10.1029/2006WR005097.

Lambot, S., E. Slob, D. Chavarro, M. Lubczynski, and H. Vereecken. 2008. Measuring soil surface water content in irrigated areas of southern Tunisia using full-waveform inversion of proximal GPR data. Near Surf. Geophys. 6:403–410.

Manfreda, S., M.F. McCabe, M. Fiorentino, I. Rodriguez-Iturbe, and E.F. Wood. 2007. Scaling characteristics of spatial patterns of soil moisture from distributed modelling. Adv. Water Resour. 30:2145–2150.

Martínez, G., K. Vanderlinden, J.V. Giráldez, and J.L. Muriel. 2009. Geophysical characterization of soil moisture spatial patterns in a tillage experiment. Geophys. Res. Abstr. 11:EGU2009-3386-15.

McCutcheon, M.C., H.J. Farahani, J.D. Stednick, G.W. Buchleiter, and T.R. Green. 2006. Effect of soil water on apparent soil electrical conductivity and texture relationships in a dryland field. Biosyst. Eng. 94:19–32.

Minasny, B., A.B. McBratney, and B.M. Whelan. 2005. Vesper: Variogram estimation and spatial prediction plus error. Available at www.usyd.edu.au/agriculture/acpa/software/vesper.shtml (accessed 1 Nov. 2009; verified 31 July 2010). Australian Centre for Precision Agriculture, Univ. of Sydney, NSW.

Mualem, Y., and S.P. Friedman. 1991. Theoretical prediction of electrical conductivity in saturated and unsaturated soil. Water Resour. Res. 27:2771–2777.

Nadler, A. 2005. Methodologies and the practical aspects of the bulk soil EC ($\sigma_a$)–soil solution EC ($\sigma_w$) relations. Adv. Agron. 88:273–312.

Or, D., and T.A. Ghezzehei. 2002. Modeling post-tillage soil structural dynamics: A review. Soil Tillage Res. 64:41–59.

Reedy, R.C., and B.R. Scanlon. 2003. Soil water content monitoring using electromagnetic induction. J. Geotech. Geoenviron. Eng. 129:1028–1039.

Remy, N., A. Boucher, and J. Wu. 2009. Applied geostatistics with SGeMS: A user's guide. Cambridge Univ. Press, Cambridge, UK.

Rhoades, J.D., P.A.C. Raats, and R.J. Prather. 1976. Effects of liquid-phase electrical conductivity, water content, and surface conductivity on bulk soil electrical conductivity. Soil Sci. Soc. Am. J. 40:651–655.

Robinson, D.A., A. Binley, N. Crook, F.D. Day-Lewis, T.P.A. Ferré, V.J.S. Grauch, et al. 2008. Advancing process-based watershed hydrological research using near-surface geophysics: A vision for, and review of, electrical and magnetic geophysical methods. Hydrol. Processes 22:3604–3635.

Robinson, D.A., I. Lebron, B. Kocar, K. Phan, M. Sampson, N. Crook, and S. Fendorf. 2009. Time-lapse geophysical imaging of soil moisture dynamics in tropical deltaic soils: An aid to interpreting hydrological and geochemical processes. Water Resour. Res. 45:W00D32, doi:10.1029/2008WR006984.

Rodriguez-Iturbe, I. 2000. Ecohydrology: A hydrologic perspective of climate–soil–vegetation dynamics. Water Resour. Res. 36:3–9.

Soil Survey Staff. 1999. Soil Taxonomy: A basic system of soil classification for making and interpreting soil surveys. 2nd ed. Agric. Handbk. 436. U.S. Gov. Print. Office, Washington, DC.

Tallon, L.K., and B. Si. 2003. Representative soil water benchmarking for environmental monitoring. J. Environ. Inf. 4:28–36.

Topp, G.C., J.L. Davis, and A.P. Annan. 1980. Electromagnetic determination of soil water content: Measurements in coaxial transmission lines. Water Resour. Res. 16:574–582.

Vachaud, G., A.P. Desilans, P. Balabanis, and M. Vauclin. 1985. Temporal stability of a spatially measured soil water probability density function. Soil Sci. Soc. Am. J. 49:822–828.

Vereecken, H., J.A. Huisman, H. Bogena, J. Vanderborght, J.A. Vrugt, and J.W. Hopmans. 2008. On the value of soil moisture measurements in vadose zone hydrology: A review. Water Resour. Res. 44:W00D06, doi:10.1029/2008WR006829.

Weihermüller, L., J.A. Huisman, S. Lambot, M. Herbst, and H. Vereecken. 2007. Mapping the spatial variation of soil water content at the field scale with different ground penetrating radar techniques. J. Hydrol. 340:205–216.

Western, A.W., R.B. Grayson, and G. Bloschl. 2002. Scaling of soil moisture: A hydrologic perspective. Annu. Rev. Earth Planet. Sci. 30:149–180.